5-1-2018

Investigation of elastoplastic ratchetting behavior of Stainless Steel 316 under cyclic uniaxial asymmetric loading at room temperature

Sirui Li
Lehigh University, sil316@lehigh.edu

Investigation of elastoplastic ratchetting behavior of Stainless Steel 316 under cyclic uniaxial asymmetric loading at room temperature

by

Sirui Li

Presented to the Graduate and Research Committee

of Lehigh University

in Candidacy for the Degree of

Master of Science

in

Mechanical Engineering and Mechanics

Lehigh University

May 2018

This thesis is accepted and approved in partial fulfillment of the requirements for the Master of Science.

_____

Date

_____

Thesis Advisor

_____

Co-Advisor

_____

Chairperson of Department

Acknowledgements

I would first like to thank my advisor Professor Natasha Vermaak for providing me a chance to do research and guiding me through my thesis. Natasha Vermaak, I really appreciate your support on this work, and I also appreciate that you steer me in the right direction. To Ali and Soner, who are members of Professor's Vermaak's lab, I cannot thank you more for the guidance and instruction you have given me while writing this thesis. Finally, I would like to thank my parents, Xi and Jian, for the encouragement and emotional and financial support you have provided me over my years as a student at Lehigh University. I have to say that without your help, I could not complete this thesis.

Contents

List of Tables

List of Figures

Abstract

This work investigates, both experimentally and computationally the cyclic behavior of stainless steel 316 under uniaxial loading at room temperature. Elastoplastic investigations of SS 316 are important in the development of an understanding of the possible behavior and their contribution to the material performance under cyclic loading. Cyclic plasticity can occur in an SS 316 component or structure depending on the loading conditions. Therefore, it is vital that the cyclic behavior of SS 316 is recognized and understood. In particular SS316 cylindrical rods specimens were tested under uniaxial cyclic loading. The experimental results show that ratchetting behavior regimes exist under the conditions presented. In order to simulate the experiments, an elastoplastic material model based on the Chaboche model is utilized in the commercial finite element (FE)-software ABAQUS. The Chaboche constitutive model utilized for cyclic loading, which includes nonlinear kinematic and isotropic hardening is discussed in detail. The kinematic and isotropic hardening parameters for the Chaboche model are also identified. The kinematic hardening parameters are calibrated using experimental data from the first half-cycle of loading, and the isotropic hardening parameters are defined by using cyclic experimental data from a test with symmetric strain (up to 1%). A 2D axisymmetric model is created in ABAQUS, where the same geometry, boundary conditions and loading cases are applied as those recorded experimentally. A mesh sensitivity study is also carried out. The error between simulation and experimental results is calculated and sources for the error are discussed. One strategy to decrease the numerical error is applied and evaluated. This work provides evidence that the Chaboche model can predict the cyclic behavior of stainless steel 316. However, there remain significant questions about the accuracy of the model parameters identified as they lead to errors in the predicted plastic strain at large cycle numbers. It is

concluded that an improved method for calibrating the parameters or a more complex constitutive model is needed to better predict the cyclic behavior of stainless steel 316.

Chapter 1

Introduction

Stainless steel (SS) 316 is an austenitic chrome-nickel stainless steel that is heat-resistant and offers superior corrosion resistance over other chromium-nickel steels when exposed to a wide range of chemical etchants and marine environments [1]. It is considered the second most common grade of steel in the stainless steel family after SS 304. SS 316 stainless steel is also known as marine grade stainless; the alloy addition of molybdenum gives corrosion resistance in reducing acids and against pitting attack in chloride solutions. Stainless steel's resistance to corrosion and staining make it an ideal material for many applications.

As SS 316 is used widely in all types of structures, its fatigue strength must be considered during design [2-4]. Due to complex loading conditions, cyclic plasticity can occur in machined SS 316 due to external discontinuities such as holes and notches and internal defects such as pores, as well as near cracks [5]. Therefore, a deep understanding of the elastoplastic performance of SS 316 under cyclic loading is required for accurate design and structural integrity.

Inelastic material behavior in closed and repeated loading paths is known as cyclic plasticity [6]. When a material is subjected to cyclic loading (loading followed by unloading and subsequent reloading, for example earthquake loading), the material response also changes cyclically until it saturates (Figure 1.1). A number of related phenomena have been observed by experiment, such as the Bauschinger effect, cyclic hardening/softening and mean stress relaxation and ratchetting [6]. Cyclic hardening or softening is

one of the most significant characteristics in cyclic plasticity, and extensive research has been carried out to better understanding the low-cycle fatigue and the plastic behavior of metals under cyclic loading [7]. Accurately simulating cycling inelasticity is an important consideration in the fatigue design since it can significantly affect fatigue life [9]. Phenomena like ratchetting (strain accumulation under stress-controlled cyclic loading with non-zero mean stress), can cause additional damage, resulting in shorter fatigue life [10].

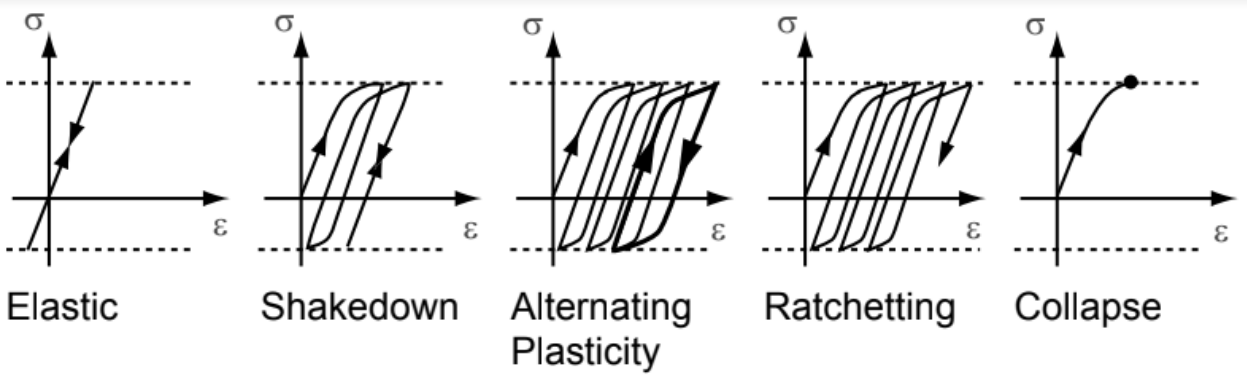

Figure 1.1: Different responses of a structure to complex cyclic loading [13]

In addition, for detailed plastic analysis of materials under cyclic loading, we need a constitutive model which can accurately describe and predict the cyclic behavior of structural components [8]. Various models have been created for simulating the cyclic behavior of materials. Prager [11] proposed a model to predict the translation of the yield surface. Another popular nonlinear kinematic hardening model, the Armstrong and Frederick model, has been successful in predicting the multiaxial Bauschinger effect associated and ratchetting strains [12]. The Armstrong and Frederick model is used extensively by Chaboche, wherein a dynamic recoil term is introduced [13]. The Chaboche model is widely available in FINITE ELEMENT (FE) software codes and it often shows an excellent correlation with experimental results for monotonic and cyclic loading [1].

The Chaboche model is one of the most widely used plasticity models for metals under cyclic loading. In reference [1], the Chaboche model was used to simulate the cyclic behavior of SS 316L (low carbon). It is concluded that the simulation with the Chaboche model only provides a very limited

description of the material behavior under cyclic loading. In reference [6], they applied Chaboche model to simulate behavior of SS 316 under strain-controlled loading conditions, and the simulation matches the experimental data very well. In this thesis, we apply Chaboche model to predict the cyclic behavior of SS 316 under stress-controlled test and assess this model's ability to capture the cyclic ratchetting behavior of SS 316 under ambient uniaxial loading conditions.

The rest of the thesis is organized as follows. Chapter 2 gives the experimental data for SS 316 under different cyclic loading conditions. In Chapter 3, the Chaboche Nonlinear Kinematic Hardening material model is explained, the parameters in this model are identified, and the method for calibrating the parameters is described. In Chapter 4, we focus on simulation. We firstly create an axisymmetric 2D model in ABAQUS, and apply the same geometry, boundary conditions and loading cases as in the experiments. Then the identified parameters are used in the constitutive model in ABAQUS. A mesh sensitivity study is also carried out. The simulations and experimental results are compared and directions for model improvement are identified and discussed. Finally, Chapter 5 continues discussion of the findings and open questions in this thesis and ends with conclusions and future directions.

Chapter 2

Experimental Results

2.1 Test Samples

The material used in the experiments performed was Stainless Steel 316 with properties shown in Table 2.1. The test specimen geometry is given in Figure 2.1.

Young's Modulus, GPa	Tensile Strength, MPa	Yield Stress, MPa	Elongation %	Hardness, Rockwell B	Hardness, Brinell Max
82.2	483	170	40	95	217

Table 2.1 Mechanical properties of SS 316[1]

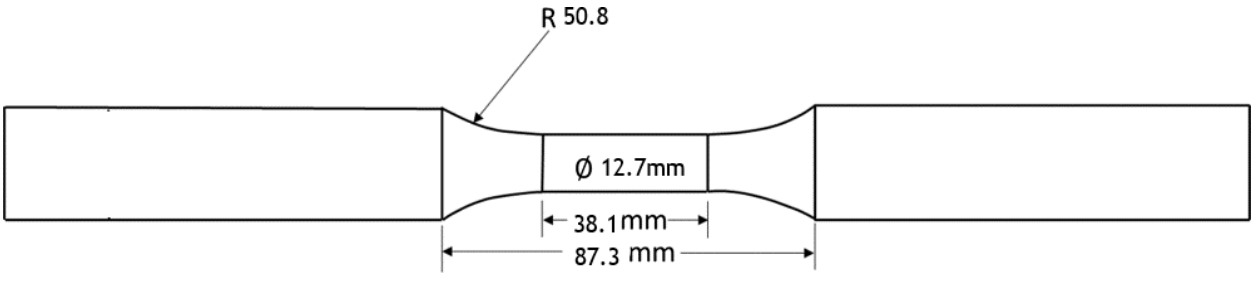

Figure 2.1 Stainless Steel 316 test sample geometry (cylindrical rod)

2.2 Loading Cases

A MTS servohydraulic test machine was used to perform uniaxial mechanical testing under tensile (monotonic) and cyclic loading conditions (stress-controlled).

Tensile tests were performed to characterize the monotonic behavior of Stainless Steel 316, and the stress-strain curve of these tensile tests is the foundation for calculating the parameters in the constitutive model described in Chapter 3.

In a strain-controlled test, the test is conducted in such a way that the strain increases at a given rate. Generally, the specimen is tested at a uniform strain rate (0.4% per second). For this thesis, symmetric strain-controlled tests at 1% strain were conducted. The results were used to record the hysteretic stress–strain response and to assess the degree of cyclic hardening or softening in the tested specimens.

In stress-controlled tests, the force is increased at a given rate. Usually, the rate of increase of the force is maintained constant. For this thesis, asymmetric stress-controlled tests were conducted. The loads applied to the specimen in the stress-controlled tests are outlined in Table 2.2, with the following definitions:

1) σ_{min} is the minimum stress.
2) σ_{max} is the maximum stress.
3) σ_{α} is the stress amplitude, given by

$$\sigma_{\alpha} = \frac{|\sigma_{max}|+|\sigma_{min}|}{2}, \tag{2.1}$$

4) σ_m is the mean stress, given by

$$\sigma_m = \frac{|\sigma_{max}|-|\sigma_{min}|}{2}, \tag{2.2}$$

σ_{min}	σ_{max}	σ_{α}	σ_m
-170.1	230.1	200.1	30

Table 2.2 Load cases used in the asymmetric stress-controlled tests

2.3 Mechanical Testing Results

Here we present three tests: (i) a tensile test, (ii) a strain-controlled test and (iii) a stress-controlled test. The data from the tensile test is used to calculate Chaboche kinematic hardening parameters and the data from the strain-controlled test is applied to calculate Chaboche isotropic hardening parameters, which will be defined and discussed in Chapter 3. These parameters are part of the constitutive model in ABAQUS that we use to simulate the stress-controlled test with the same loading conditions as in the experiment. Then we compare the stress-controlled experimental loading cases with our simulations (using the parameters found from the strain-controlled tests) to assess the utility of the Chaboche model.

2.3.1 Tensile Test

The SS 316 material properties determined from the tensile test are presented in Figure 2.2, where E is the Young's modulus and σ_y is the 0.2% proof stress. The value of the 0.2% proof stress is set at 0.2% plastic strain and it will be used to calculate the parameters in the constitutive model (Chapter 3).

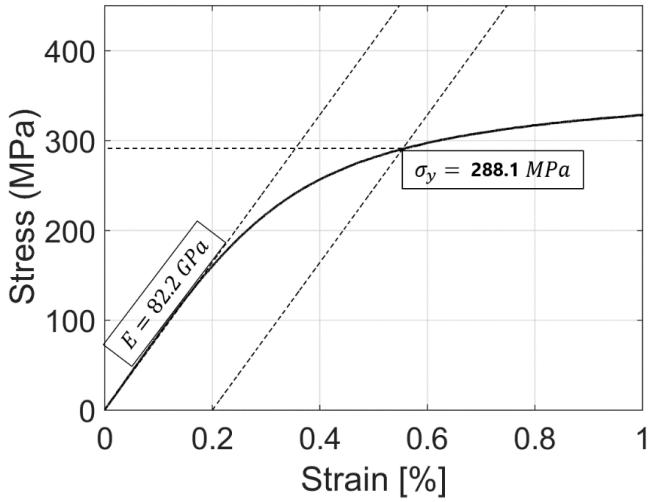

Figure 2.2 Tensile properties of SS 316, determined experimentally

2.3.2 Symmetric Strain-Controlled Test

The stress-strain data for the symmetric strain-controlled load case is presented in Figure 2.3. In this experiment, 200 cycles were performed.

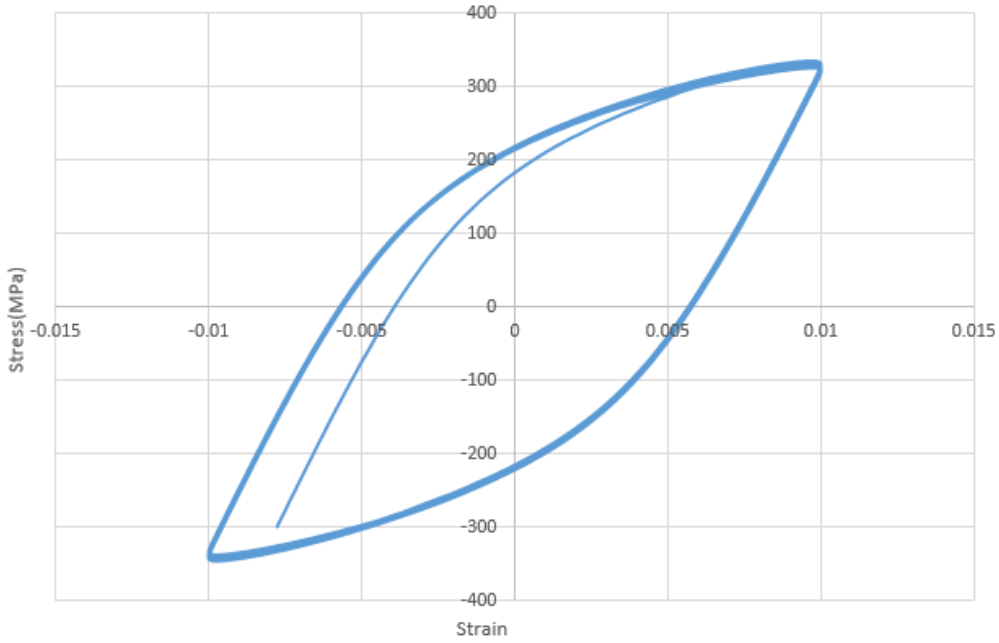

Figure 2.3 Hysteresis loops for the SS316 symmetric strain-controlled

2.3.3 Asymmetric Stress-Controlled Test

Figure 2.4 presents the changing shape of the hysteresis loops at various cycle counts. The ratchetting (strain accumulation) phenomena can be clearly distinguished in this graph after the 180th cycle. The ratchetting strains obtained from the stress-controlled test are also presented in Figure 2.5.

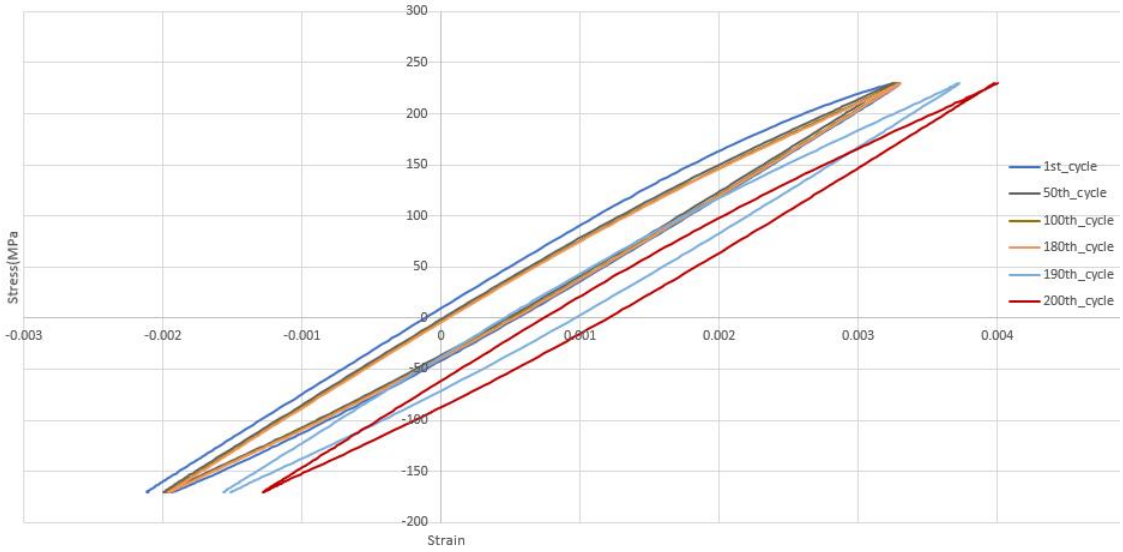

Figure 2.4 Experimental data for SS316 showing the hysteresis loop progression

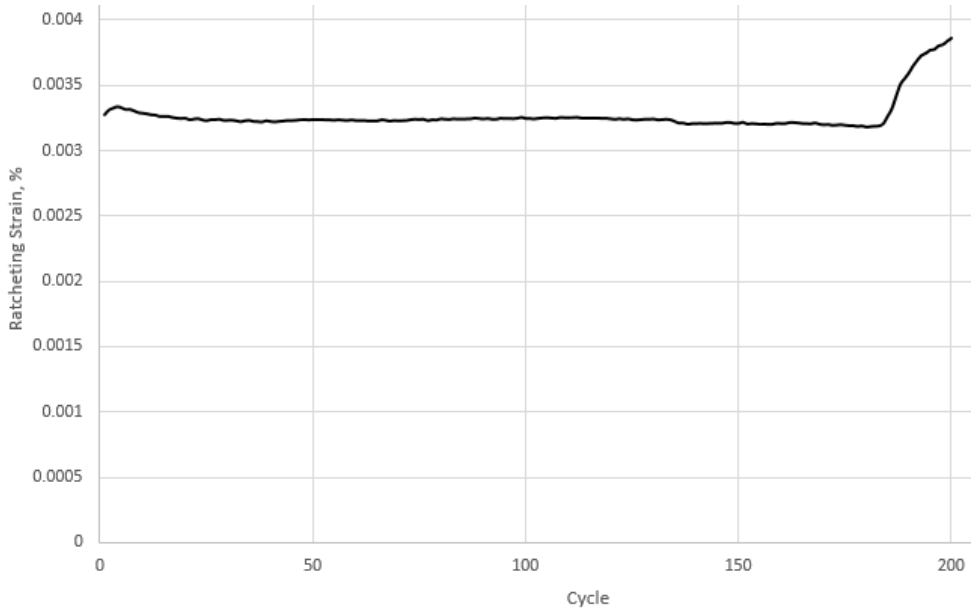

Figure 2.5 Ratchetting strain curve (points correspond to strain at the peak of each loading cycle)

We can note that the hysteresis loops before the 184th cycle are nearly stable and the total strain does not change until the 184th cycle. As ratchetting is a significant phenomenon for asymmetrical stress cycling, it is important in designing structural components [14]. Thus to focus on ratchetting, we focus on

the cycles from 184th to 200th. Figure 2.6 shows the ratchetting strain curve between the 184th cycle and 200th cycle.

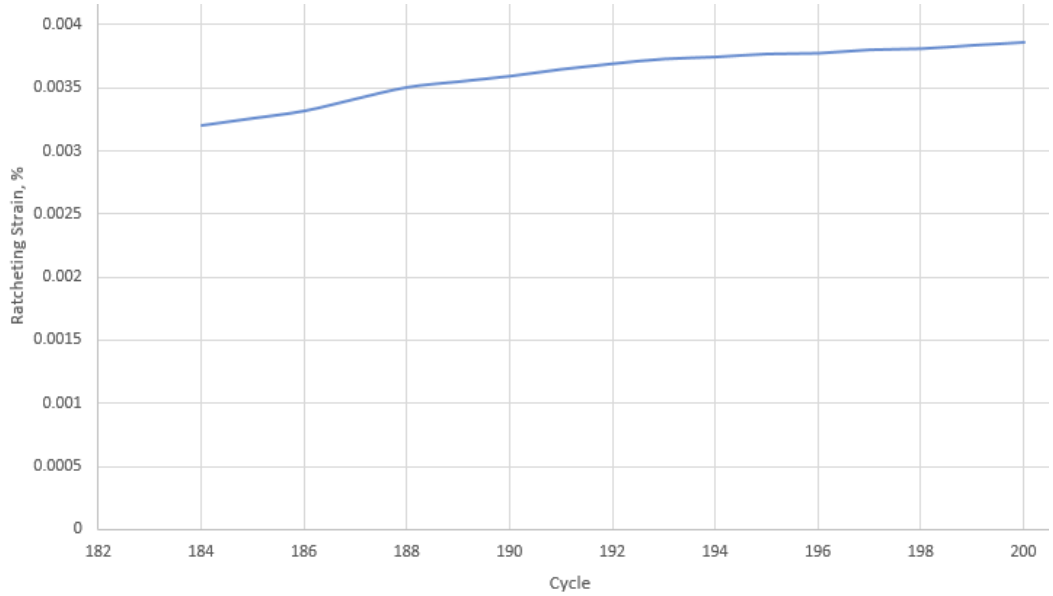

Figure 2.6 Ratchetting strain curve after the 180th cycle

From Figure 2.6 we can see that the total strain increases and the rate of accumulation decreases after the 188th cycle (the increasing of total strain from 194th to 200th is only 3%). The stabilization of the maximum strain per cycle in the results presented in Figure 2.6 provides evidence of alternating plasticity behavior. Alternating plasticity behavior is one in which the steady state is a closed elastic-plastic loop, with no net accumulation of plastic deformation. The plastic strain increment obtained during the first half of each loading cycle is followed by a plastic strain increment of equal magnitude but opposite sign during the second half. The saturation of ratchetting strain is very important especially when it comes to fatigue calculation.

Chapter 3

Constitutive Model

Many elastoplastic material models are proposed to simulate and predict the cyclic loading behavior of metals. The Prager model, proposed in 1956, often over-predicts ratchetting responses at the beginning of cycling, which can be followed by shakedown upon further cycling [15]. The nonlinear kinematic hardening model of Armstrong and Frederick (1966) also over predicts ratchetting strains for uniaxial loading, which is mentioned in their study [15]. However, it has been found and reported in the literature that other nonlinear kinematic models like the Chaboche model are well suited for cyclic loading, especially for showing ratchetting behavior. This is because the Chaboche model is better able to capture yield surface translation during cyclic loading.

In this Chapter, the Chaboche constitutive model for cyclic loading, which includes both nonlinear kinematic and isotropic hardening, is discussed in detail (Figure 3.1). In general, a kinematic hardening rule can use a translating yield surface to capture transient cyclic phenomena, whereas isotropic hardening rules attempt to use expansion of the yield surface to model cyclic hardening or softening [9].

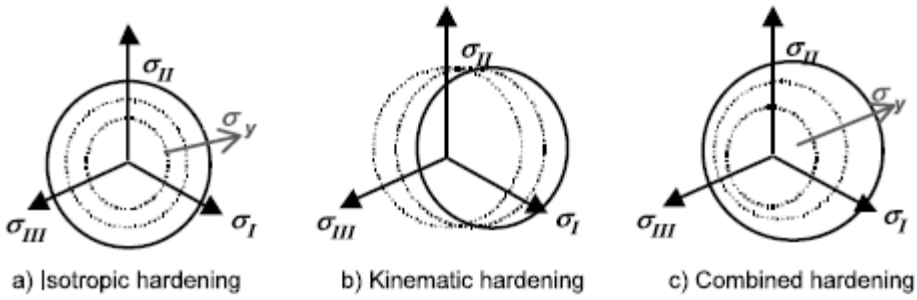

Figure 3.1: Yield surface modification with plastic deformation in the principal stress space. Isotropic, kinematic and combined hardening [16]

3.1 Mathematical Formulation

The Chaboche model is formulated starting from the assumption of additive decomposition of the strain tensor (ε):

$$\varepsilon = (\varepsilon^e + \varepsilon^p), \tag{3.1}$$

Here ε is the total strain, and ε^e and ε^p are the elastic and plastic parts respectively. Hooke's law (the linear elastic relationship between stress and strain) can then be written:

$$\sigma = D{:}(\varepsilon - \varepsilon^p), \tag{3.2}$$

where σ is the true stress and D is the 4th order elastic stiffness tensor and taken to be the Young's modulus (E) for the material. The yield function used in the current model is a von Mises yield function. The yield function F is a function of the back stress α (location of the center of the yield surface), s (the deviatoric component of the stress tensor), and σ_0 (current yield stress). It can be written:

$$F = \sqrt{\frac{3}{2}(s-\alpha)(s-\alpha)} - \sigma_0 = 0, \tag{3.3}$$

The associated flow rule is:

$$\lambda = |\dot{\varepsilon}^p| = \sqrt{\frac{2}{3} d\varepsilon^p : d\varepsilon^p}, \tag{3.4}$$

where $\boldsymbol{\lambda}$ is the plastic strain evolution and $d\varepsilon^p$ is the plastic strain increment.

Next, the hardening rule should be considered. At the continuum level, hardening is presented as the change of the yield surface location in stress space as the plastic strain increasing [17]. There are two types of hardening rules, isotropic hardening and kinematic hardening. This model includes a combined isotropic-kinematic hardening formulation, which was first introduced by Armstrong and Frederick, and then modified by Chaboche. For the kinematic hardening, the hardening law is:

$$\dot{\alpha} = \sum_{i=1}^{n} \dot{\alpha}_i = \sum_{i=1}^{n} (\frac{2}{3} C_i d\varepsilon^p - \gamma_i \alpha_i \lambda), \tag{3.5}$$

where n is the number of backstresses, α is the backstress, (which represents the displacement of the center of the yield surface), and C and γ are material parameters that must be calibrated from cyclic test data(the details for this calibration are presented in Chapter 3.2). In particular, C is the initial kinematic hardening moduli, and γ determines the rate at which the kinematic hardening moduli decrease with increasing plastic deformation.

For isotropic hardening, the exponential Voce's formula is introduced:

$$\sigma^0 = \sigma_0 + Q_\infty (1 - e^{-b\bar{\varepsilon}^{pl}}), \tag{3.6}$$

where σ^0 represents the evolution of the yield surface size, σ_0 is the yield stress at zero plastic strain, $\bar{\varepsilon}^{pl}$ is the equivalent plastic strain (we will explain how to calculate it later), Q_∞ is the maximum change in the size of the yield surface, and b defines the rate at which the size of the yield surface changes as plastic straining develops, both of which can be calculated from experimental data.

From the above equations, a set of parameters needs to be determined when nonlinear kinematic hardening and isotropic hardening are considered. The unknown parameters are:

σ_0 = initial yield stress

C_i and γ_i = kinematic hardening parameters

Q_∞ and b = isotropic hardening parameters

These parameters must be calibrated and imported into ABAQUS for simulations.

3.2 Parameter Identification

3.2.1 Defining the Isotropic Hardening Component

Isotropic hardening can be introduced by specifying the equivalent stress defining the size of the yield surface, σ^0, as a tabular function of the equivalent plastic strain [22]. The simplest way to obtain this data is to conduct a symmetric strain-controlled cyclic experiment with a strain range $\Delta\varepsilon$ (Figure 3.2). Since the material's elastic modulus is large compared to its hardening modulus, this experiment can be interpreted approximately as repeated cycles over the same plastic strain range:

$$\Delta\varepsilon^{pl} \approx \Delta\varepsilon - 2\sigma_1^t/E, \tag{3.7}$$

where E is the Young's modulus, and σ_1^t is the peak tensile stress in the first cycle.

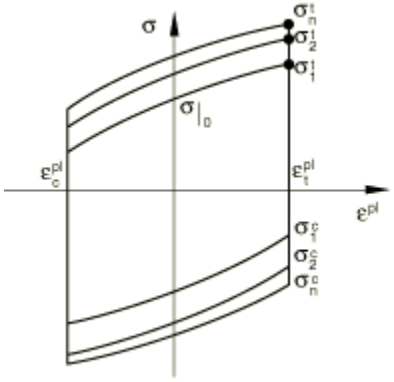

Figure 3.2: Schematic of symmetric strain cycle experiment used to find model parameters

The equivalent stress defining the size of the yield surface is σ_0 at zero equivalent plastic strain; for the peak tensile stress points, the equivalent stress is obtained by isolating the kinematic component from the yield stress:

$$\sigma_i^0 = \sigma_i^t - \alpha_i, \tag{3.8}$$

Since the model predicts approximately the same backstress value in each cycle at a particular strain level, the backstress α_i for each cycle i is:

$$\alpha_i \approx (\sigma_1^t + \sigma_1^c)/2, \tag{3.9}$$

The equivalent plastic strain corresponding to σ_i^0 is:

$$\bar{\varepsilon}_i^{pl} = \frac{1}{2}(4i - 3)\Delta\varepsilon^{pl} \tag{3.10}$$

Data pairs (σ_i^0, $\bar{\varepsilon}_i^{pl}$), including the value σ_0 at zero equivalent plastic strain, are specified in tabulated form. The tabulated values defining the size of the yield surface should be provided for the entire equivalent plastic strain range to which the material may be subjected [18].

In this thesis, we choose a strain range of $\pm 1\%$, and by using the method above we can get 7 pairs of (σ_i^0, $\bar{\varepsilon}_i^{pl}$) as below:

σ_i^0	$\bar{\varepsilon}_i^{pl}$
169.3930454	0
169.689769	0.007895863
171.4695261	0.071062771
172.3110744	0.134229678
172.8697252	0.22898004
173.170717	0.292146947
173.7091448	0.513231123
173.9414349	0.702731845

Table 3.1 Input for isotropic parameters calculations

Now that we have equation 3.6 and the data in Table 3.1 above, we can apply a curve fit function in Matlab (Figure 3.3) to obtain the Parameters Q_∞ and b.

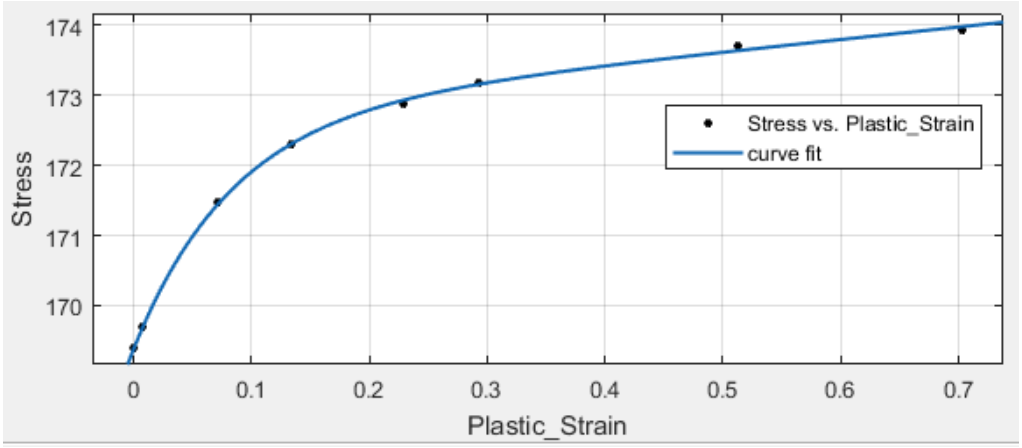

Figure 3.3 Curve Fit for isotropic parameters

The result is:

$$Q_\infty = 3.355$$

$$b = 12.04$$

3.2.2 Defining the Kinematic Hardening Component

C and γ can be based on the stress-strain data obtained from the first half cycle of a unidirectional tension or compression experiment. The monotonic stress–strain curve is the basis for the calibration process. First, we need to translate the true stress and strain to engineering stress and strain by:

$$\varepsilon = \exp(\varepsilon_{true}) - 1 \tag{3.11}$$

$$\sigma = \sigma_{true}/(1 + \varepsilon) \tag{3.12}$$

The stress strain curve up to 1% total strain is shown in Figure 3.4. The calibration is most effective when limited to the strain regime that is anticipated in the application (e.g. 5%) and this avoids the necessity to perform curve fitting of the backstress beyond that strain regime [19]. Furthermore, many standards (ASME [21], etc.) determine that the maximum allowable plastic strain accumulation should be less than 5%.

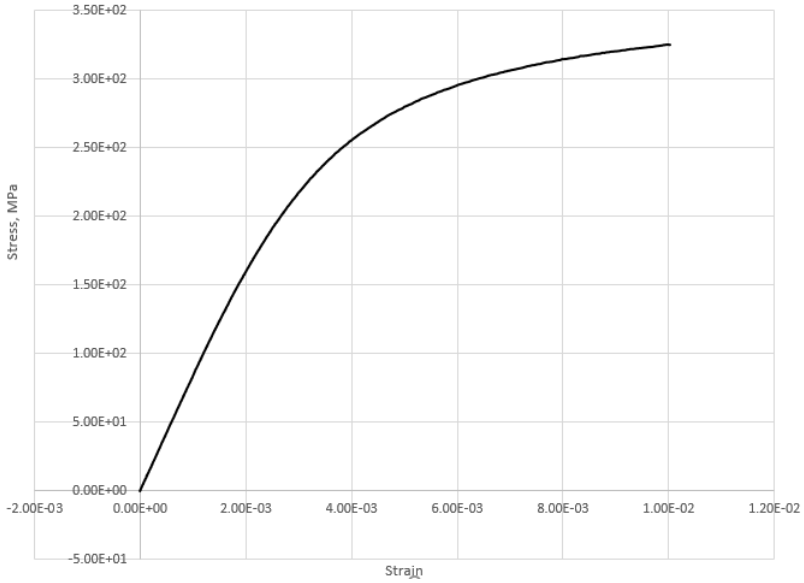

Figure3.4 Stress-strain curve up to 1% strain

The backstress and the kinematic parameters are based on the stress-plastic strain curve. To get the calibration curve in Figure 3.5, the elastic limit and yield stress were first determined. The elastic limit for stainless steel is difficult to determine since it depends on the accuracy of the instrumentation (strain gauge, digital extensometer, etc.). Therefore, it is recommended that the average 0.2% proof stress ($R_{p0.2}$) or the calculated yield stress by the 0.2% offset method (σ_y) be multiplied by a factor of 0.55 [19]. For this analysis the average of the 0.2% proof stress and the uniaxial yield stress (0.2% offset) have to be assumed. This is due to the fact that when ratchetting analysis was performed using the 0.2% offset stress, no increase in plastic strain accumulation was seen (i.e. shakedown), while when using the $R_{p0.2}$ value for yield stress, strain accumulation was over-predicted by the model.

Therefore the yield stress chosen was $\sigma_0 = (\sigma_y + R_{p0.2})/2$. At σ_0 plastic strain is set to zero. To generate the true stress-plastic strain curve needed, the offset strain at σ_0 is determined to be 0.000211. Using this strain offset, we then determine the plastic strain using the relation:

$$\varepsilon_p = \varepsilon - (\frac{\sigma}{E} + 0.00005108) \tag{3.13}$$

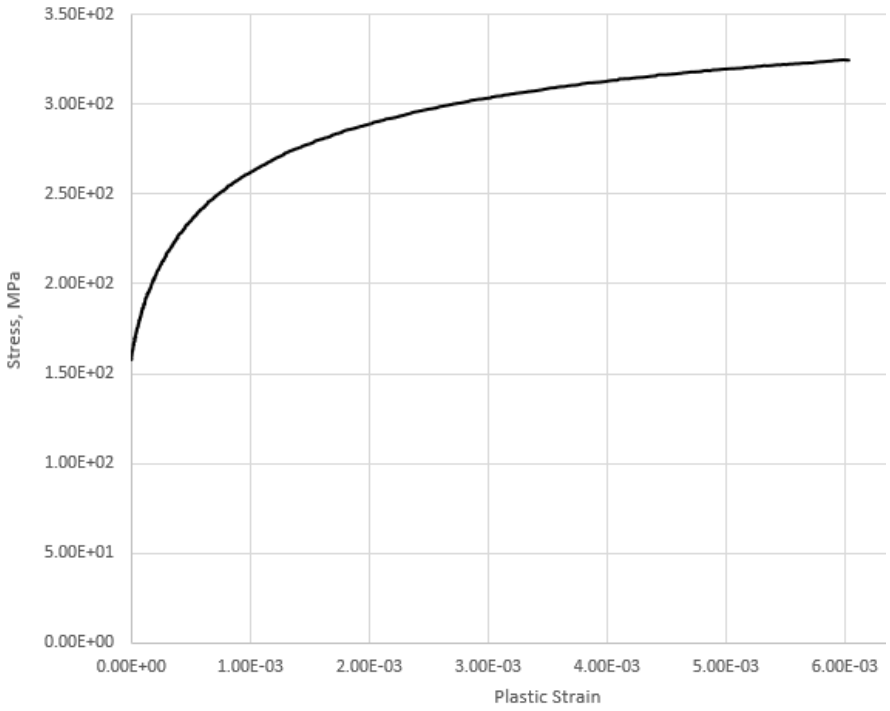

Figure 3.5 Stress-Plastic Strain curve for SS316

Next, the backstress was determined. Backstress (location of the center of the yield surface in stress space) is the vital parameter in the nonlinear kinematic (NLK) calibration process. For a one-dimensional representative of an NLK model, the backstress is determined using:

$$\alpha = \sigma - \sigma_0 \tag{3.14}$$

where σ is the uniaxial stress state and σ_0 is the initial yield stress at the elastic limit. This backstress is included in Fig. 3.6.

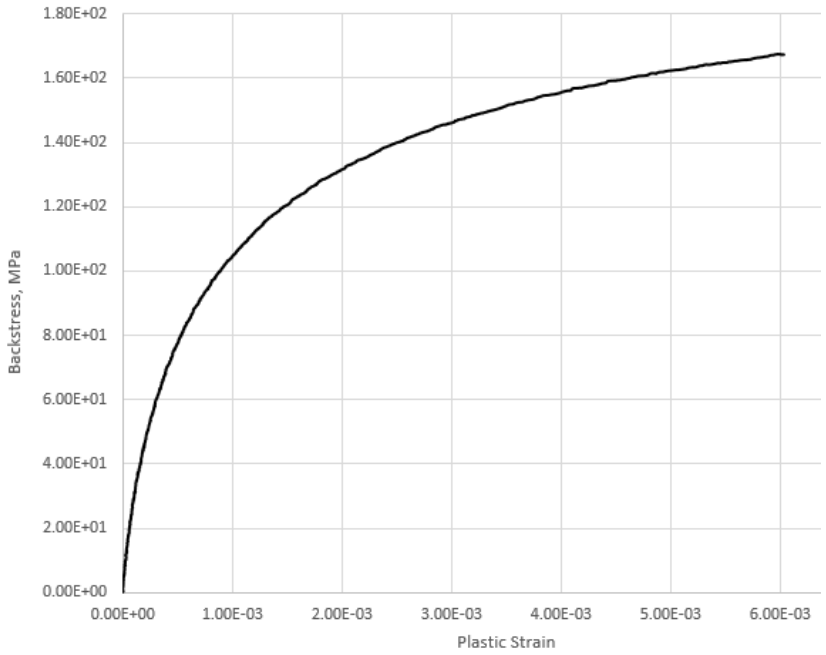

Figure 3.6 Backstress curve

Once the stress-plastic strain curve is known, the α backstress curve is also known. From equation 3.5 and the backstress curve, we can determine the parameters of the Chaboche non-linear kinematic model by one of two options. The first option is the manual method. It can be performed without any help from outside software. The details of this method are given in [19]. The second option is performed via ABAQUS automated calculation. In this second case, once the input (the stress-plastic strain data in Figure3.5) for calibration is determined, an ABAQUS input file is used to automatically calibrate the Chaboche components which are shown in Table 3.2. Material parameters for our SS 316 test specimens were specified by using the following input file lines [20], (also shown in Figure 3.7).

*PLASTIC, HARDENING=COMBINED,
DATATYPE=HALFCYCLE, NUMBER BACKSTRESSES=2,

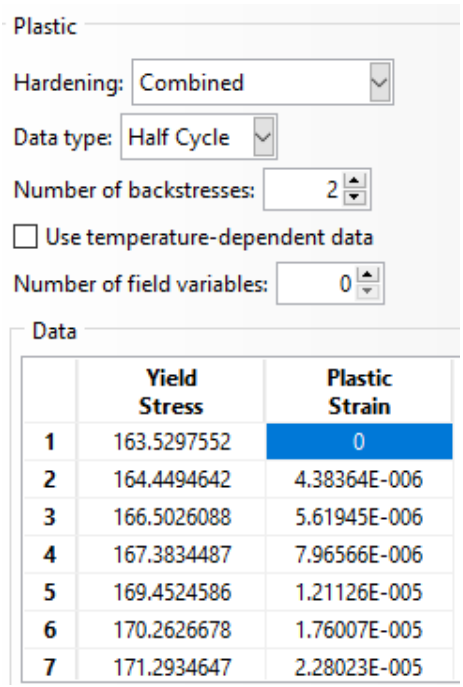

	Yield Stress	Plastic Strain
1	163.5297552	0
2	164.4494642	4.38364E-006
3	166.5026088	5.61945E-006
4	167.3834487	7.96566E-006
5	169.4524586	1.21126E-005
6	170.2626678	1.76007E-005
7	171.2934647	2.28023E-005

Figure3.7 Input file for material parameters claculations

This line is followed by the tabulated data from Figure 3.5. ABAQUS then calculates the parameters, C_k and γ_k. Two backstress components were used and they are listed in Table 3.2.

Initial Yield		163.53 (MPa)	
Chaboche component		C_k	γ_k
	1	49706	461.88
	2	234195	3736.1

Table 3.2 Chaboche parameters determined

Now that we have both kinematic hardening parameters and isotropic parameters, we can apply these parameters to create a model in ABAQUS to simulate the different phenomena observed experimentally. With good experimental agreement, the model may then be modified to investigate more complex loading scenarios (such as multiaxial loading or thermomechanical loading) or other similar

materials systems to help design additional experimental programs and understand the elastoplastic behavior. Comparison between experiments and simulations is presented in Chapter 4.

Chapter 4

Numerical Simulations in ABAQUS

The ABAQUS finite element software [18] was used to simulate the experimental conditions. In this example, deformation of a SS 316 specimen subject to cyclic loading is studied. Static analyses are performed. Taking advantage of the axial symmetry of the specimen, axisymmetric elements are used.

4.1 Geometry of the Model

The 2D axisymmetric sketch of this model, which is the same as the experimental specimens, is shown in Figure 4.1. The shape of the testing specimen is a cylindrical rod shape. All dimensions are specified in the figure in mm. The diameter at the middle is a half inch (12.7mm) which is the same size as the test samples, and the diameter at the gripping ends is one inch (25.4mm).

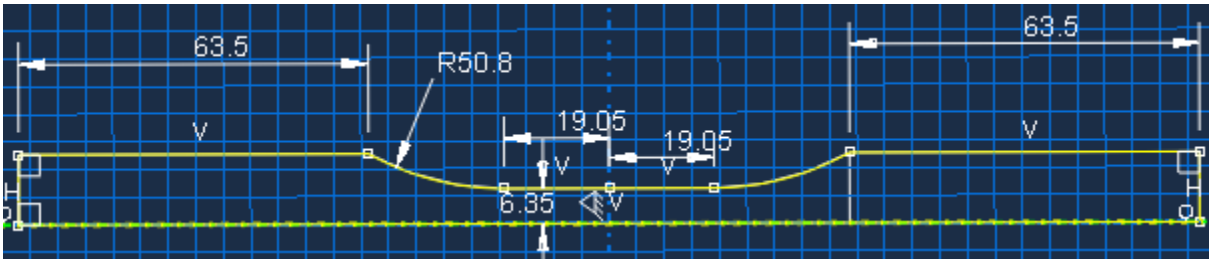

Figure 4.1 Sketch of the model

4.2 Boundary Conditions and Loading

The specimen is constrained at the bottom in the longitudinal (Y) direction, and a load is applied to the top surface. In ABAQUS, we partition the bottom part and set the bottom part as ENCASTRE (see the boundary condition settings of Figure 4.2).

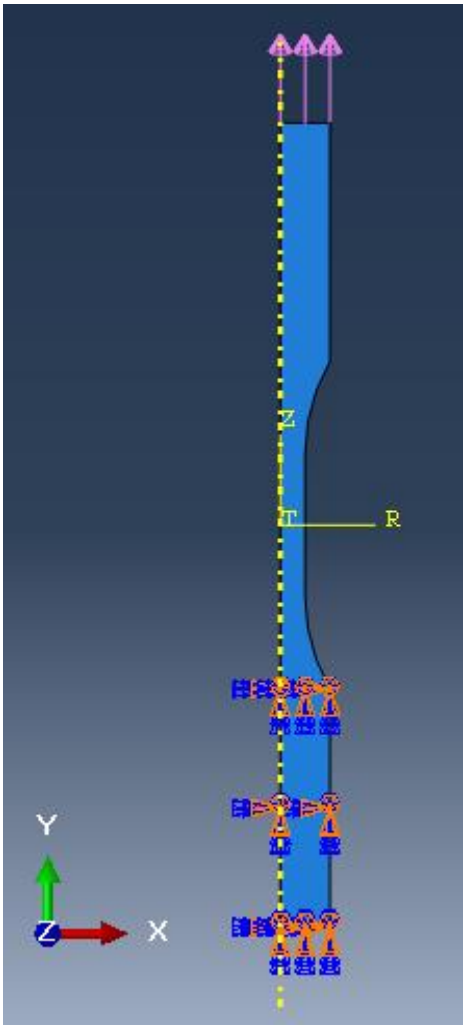

Figure 4.2 Model's boundary condition in ABAQUS

For the loading, we set the type of the loading as uniform pressure. Since the cross-sectional area in the center is one quarter of the top surface, the magnitude of the pressure should be multiplied by 0.25. The cyclic loading of $\sigma_m = -170.1MPa$ and $\sigma_\alpha = 230.1MPa$ is applied to the top surface of the model. The loading case from the experiment is shown in Figure 4.3. The stress versus time is a sine or cosine

function, so we choose 20 points in each cycle to create a smooth tabular amplitude to simulate the same loading conditions.

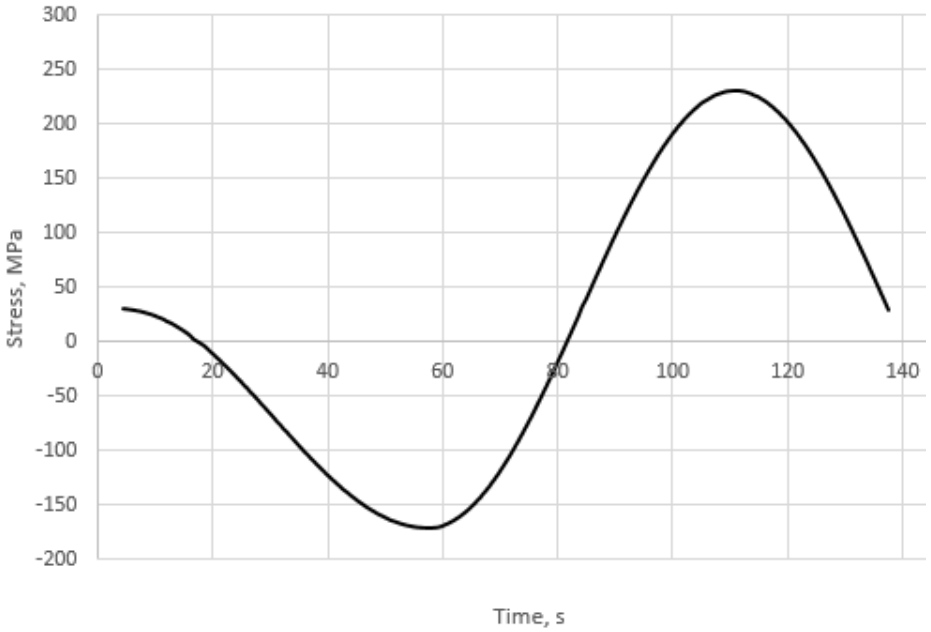

Figure 4.3 Experimental Loading versus time

4.3 Mesh Sensitivity Study

The model specimen is meshed with CAX4R and CAX3 elements. To ensure accuracy, a mesh sensitivity study is carried out. Four different sizes of approximate global seeds (shown in Figure 4.4) are applied to find a suitable mesh size (the approximate global size factors are 16, 8, 4, and 2). The four different meshes are shown in Figure 4.4.

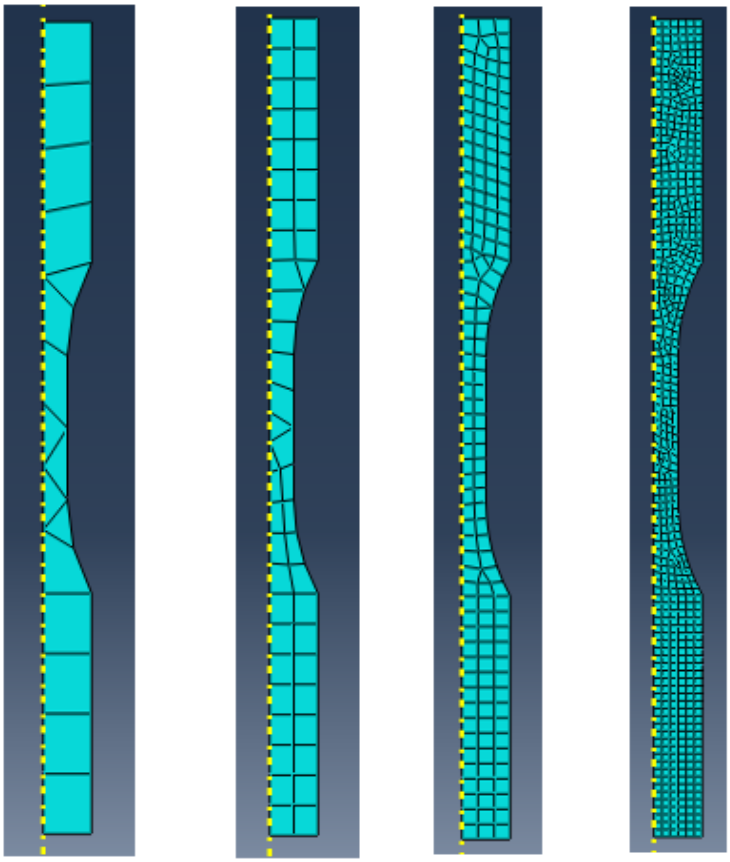

Figure 4.4 Four different mesh sizes

The monotonic loading case is applied to these four different mesh sizes and the stress-strain curve is shown in Figure 4.5.

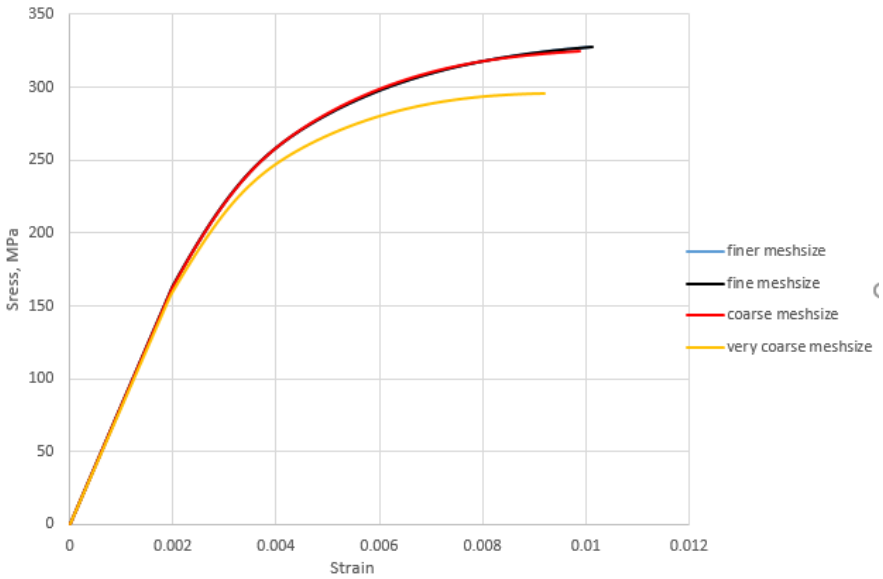

Figure 4.5 Stress-strain curve for different mesh sizes

From Figure 4.5, we can see that the results from the coarsest mesh size are very different from the other three mesh results. As the mesh size becomes finer, the stress-strain curve begins to converge and the last two curves are nearly overlapping. Based on this study, it is determined that the 3rd mesh size (approximate global size factor 4 – with CAX4R elements through the center diameter) is fine enough to complete the simulation.

4.4 Simulation Results and Discussion

First we compare the FE simulation results with experimental data under the monotonic loading case in Figure 4.6. It can be seen that the results from the FE simulation match the experiment result very well (within 3% error at most).

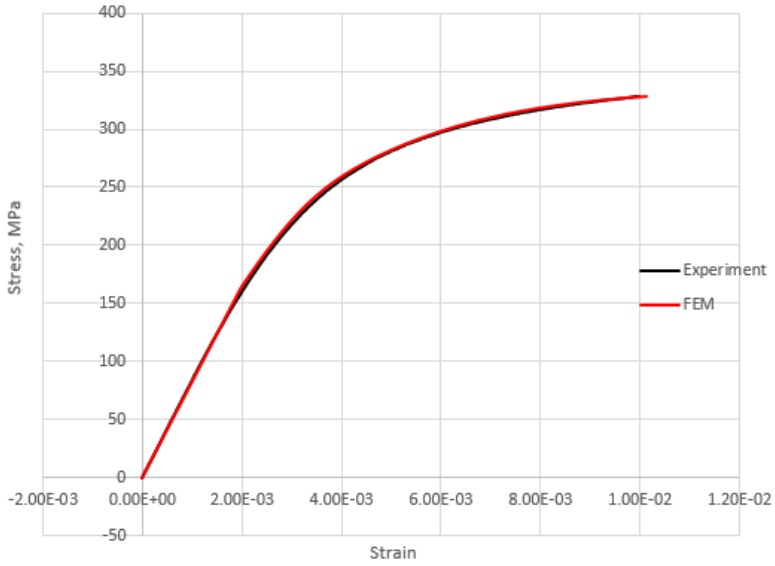

Figure 4.6 FEM and Experiment results under monotonic loading

Second, as the hysteresis loops from the cyclic loading case (see Figure 2.5) before the 184th cycle are stable and then ratchetting behavior appears after the 184th cycle. To focus on capturing ratchetting behavior, we focus on the cycles between the 184th and 200th cycle. The simulation (black) and experimental (blue) results are presented in Figure 4.7. The element positioned at the center of the model (the red point shown in Figure 4.8) is chosen to compute the stresses and strains.

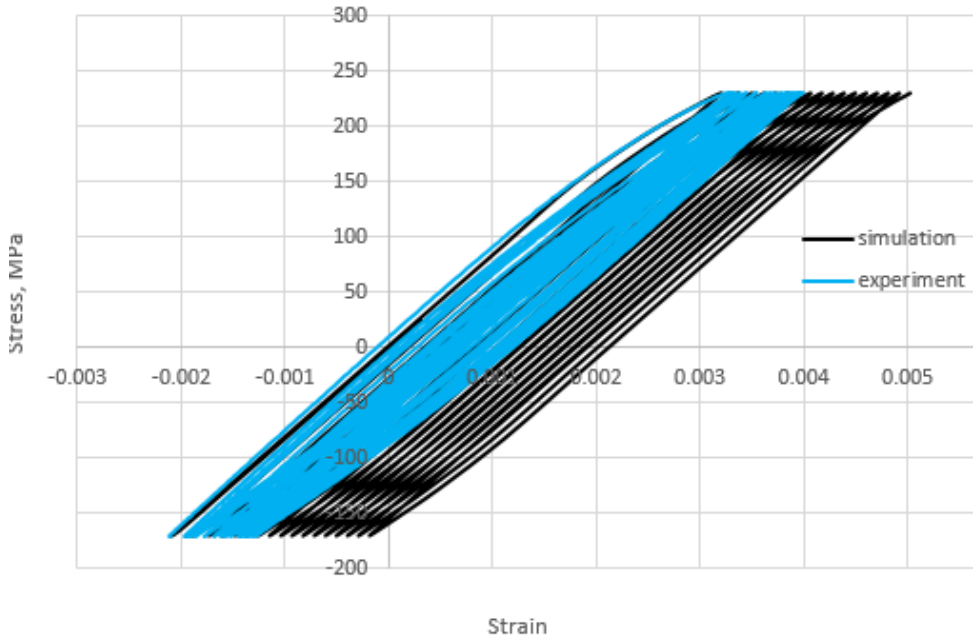

Figure 4.7 Stress-strain curve under cyclic loading

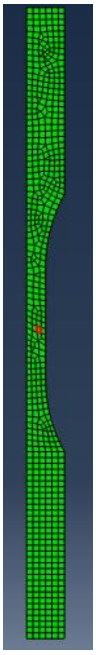

Figure 4.8 The element chosen to be analyzed

The simulation results agree with the experimental data during the first cycle, but they over-predict the strain as the number of cycles increases. The peak strain (maximum axial strain) at each cycle is reported in Figure 4.8 to better compare these results.

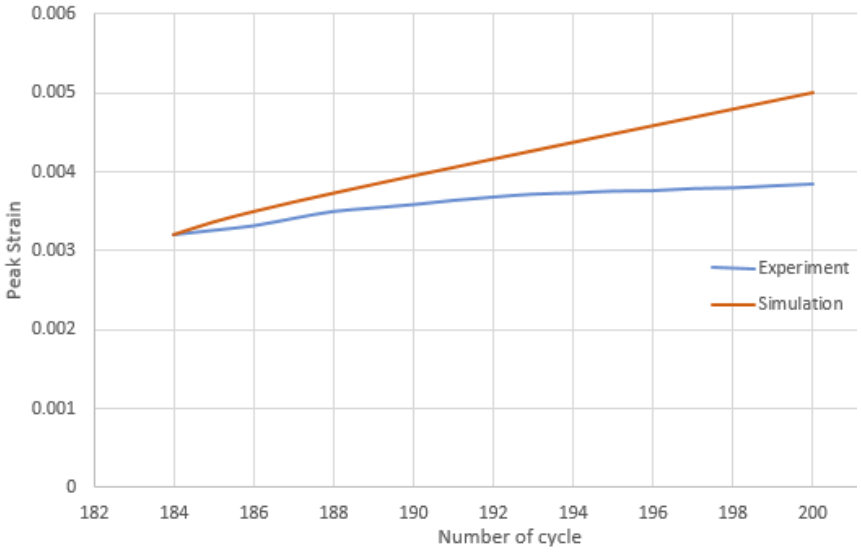

Figure 4.9 Maximum axial strain versus number of cycle

From Figure 4.9, the model shows a good prediction of the accumulated plastic strain for a small number of cycles (cycle 1 through 4). The error at the 188th cycle is only 6%. However, as the cycles continue (after the 190th cycle), the over-prediction of the accumulated strain becomes very large. The error at the 200th cycle is nearly 30%.

The transition from good agreement to large over-prediction occurs around the 188th cycle. The rate of accumulation decreases after cycle 188 and this trend is not captured by the ABAQUS simulations. The absence of the trend as the number of cycles increases may be due to the isotropic component of the NLK (related to the expansion or contraction of the yield surface in stress space). The isotropic component should be defined by specifying the equivalent stress at zero plastic strain and the evolution of the equivalent stress as a function of equivalent plastic strain as mentioned before. If this component is not defined accurately, the size of the yield surface is not well matched during cycling.

Typically, the isotropic hardening properties are more sensitive to loading conditions than kinematic hardening properties [18]. By using the method in Chapter 3, the parameters we determined were not accurate enough. This is because the actual stress versus plastic strain curve in the strain-controlled test does not look like Figure 3.2. It is very hard to find the peak compression points. The curve should be very smooth and we can only choose an approximate point to replace it. This could be

one source of error in the simulations. To investigate this potential source of error, we next modify the value of the isotropic parameters, Q_∞ and b. For example, if the value of Q_∞ is changed to 280, the results are shown in Figure 4.9.

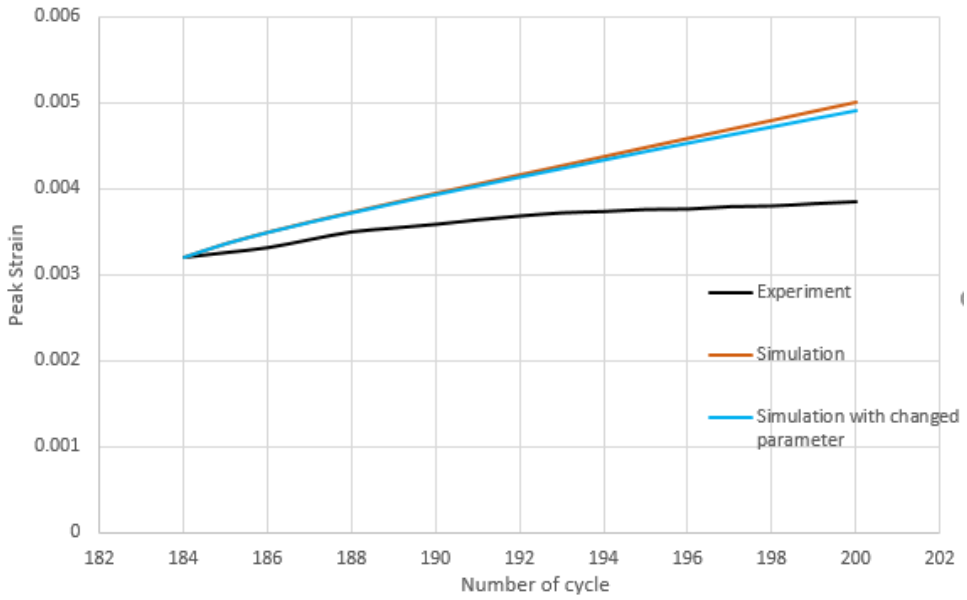

Figure 4.10 Maximum axial strain versus number of cycle with modified parameter Q_∞

The blue curve is the FE results with the modified parameters Q_∞ and original b. The new curve has nearly the same shape as the previous one but it agrees better with (although still over predicts) the experimental results. The error at the 200th cycle decreases to 27%, but it is still very high. By comparing these two FE simulation results, we can note that we could get better agreement at higher loading cycles if an alternative method or justification for determining Q_∞ (that gives a bigger value) can be found. Furthermore, it might be necessary to recalibrate the isotropic component of the Chaboche model during cyclic loading.

Chapter 5

Conclusion and Future Work

This work studies the elastoplastic behavior of stainless steel 316 under asymmetric cyclic loading. SS 316 exhibits low strain accumulation (ratchetting) and then tends to achieve shakedown upon further cycling. In order to further understand and simulate the elastoplastic behavior of this material, ABAQUS finite element analysis using the NLK material model was performed. The model was calibrated using monotonic data via a user input file according to the method described in [22]. For the loading cycles from the 1^{th} to the 188^{th}, the FE model closely matches the experimental data. However, as the number of cycles increases, decreasing of the rate of total strain accumulation does not occur and leads to large over-prediction of the ratchetting strain.

The Chaboche model used in this work can predict the cyclic behavior of stainless steel 316. However, further attention must be paid to determining suitable model parameters in order to avoid the over-prediction and nearly 30% error at the 200^{th} cycle found in this study. It is expected that the problem lies in the model calibration—in particular, difficulties were encountered in determining the transition from elastic to plastic behavior and the experimental stress-strain response was not as straightforward as presented in the directions according to the Chaboche model for parameter determination. It is difficult to find peak compression points as expected in Figure 3.2. Within this work, the evolution of the yield surface was determined in a coarse manner using experimental data. So further calibration of the isotropic component parameters of the Chaboche model may also be needed to better match experimental data. For future work, it remains to explore other accurate methods of calculating the parameters in the Chaboche

model and to better predict the cyclic behavior of stainless steel 316. One of the ways to calibrate parameters accurately is through parametric optimization. Given an initial value of parameters: C_k, γ_k, Q_∞ and b, we could systematically vary and compare FE results, until the FE results match the experimental data to within a specified level. Lastly, study of the microstructural features of the stainless steel specimen would benefit in determining changing deformation mechanisms during cycling. Alternatives to the Chaboche model that allow for more complex behavior (and more complex experiments for model calibration) may also be needed.

Bibliography

[1] van Eeten, P. and Nilsson, F. "Constant and Variable Amplitude Cyclic Plasticity in 316L Stainless Steel," Journal of Testing and Evaluation, Vol. 34, No. 4, 2006, pp. 298-311.

[2] Dutta A, Dhar S, Acharyya S.K. “Material characterization of SS 316 in low cycle fatigue loading”. J Mater Sci (2010) 45: 1782-1789.

[3] Shit J, Dhar S, Acharyya S. “Modeling and Finite Element Simulation of Low Cycle Fatigue Behavior of 316 SS”. 6th International Conference on Creep, Fatigue and Creep-Fatigue Interaction [CF-6]. Procedia Engineering 55 (2013) 774– 779.

[4] Hassan Tasnim, Kyriakides Stelios. Ratchetting in Cyclic Plasticity, Part I: Uniaxial Behavior. International journal of plasticity, vol 8, pp. 91-116, 1992.

[5] Cyclic Elastoplastic Performance of Aluminum 7075-T6 Under Strain- and Stress-Controlled Loading.” Agius, D., Wallbrink, C. & Kourousis, K.I. J. of Materi Eng and Perform (2017) 26: 5769.

[6] J. Shit, S. Dhar, S. Acharyya, “Modeling and Finite Element Simulation of Low Cycle Fatigue Behaviour of 316 SS”, Procedia Engineering, Volume 55, 2013, Pages 774-779, ISSN 1877-7058.

[7] Mroz, Z, “An Attempt to Describe the Behavior of Metals Under Cyclic Loads Using a More General Workhardening Model.” Acta Mechanica, Vol. 7, 1969, pp. 199-212.

[8] Ohno NN, Kachi YY. “A Constitutive Model of Cyclic Plasticity for Nonlinear Hardening Materials.” ASME. J. Appl. Mech. 1986;53(2):395-403. doi:10.1115/1.3171771.

[9] “Aluminum Alloy 7075 Ratchetting and Plastic Shakedown Evaluation with the Multiplicative Armstrong–Frederick Model”. Dylan Agius, Kyriakos I. Kourousis, Chris Wallbrink, Weiping Hu, Chun H. Wang, and Yannis F. Dafalias AIAA Journal 2017 55:7, 2461-2470

[10] Z. Xia, D. Kujawski, F. Ellyin, “Effect of mean stress and ratchetting strain on fatigue life of steel, International Journal of Fatigue,” Volume 18, Issue 5, 1996, Pages 335-341, ISSN 0142-1123.

[11] Prager W. (1956) “A new method of analysing stresses and strains in work hardening plastic solids.” ASME J. Appl. Mech.,23, 493 – 496.

[12] Chaboche, J.L. (1991) “On some modifications of kinematic hardening to improve the description of ratchetting effects.” Int. J. Plasticity, 7, 661 – 678.

[13] Kaddour Mouattah & Abderrahim Bali (2014) “Prediction of structural ratchetting by various models,” 28:1, 21-27, DOI: 10.3184/096034011X12962347725684

[14] Guozheng Kang, Qing Gao, Xianjie Yang, “A visco–plastic constitutive model incorporated with cyclic hardening for uniaxial/multiaxial ratchetting of SS304 stainless steel at room temperature,” Mechanics of Materials, Volume 34, Issue 9, 2002, Pages 521-531, ISSN 0167-6636.

[15] “Cyclic loading of beams based on the Chaboche model,” Shojaei, A., Eslami, M.R. & Mahbadi, H. Int J Mech Mater Des (2010) 6: 217. September 2010, Volume 6, Issue 3, pp 217–228.

[16] “The Chaboche nonlinear kinematic hardening model: calibration methodology and validation Broggiato,” G.B., Campana, F. & Cortese, L. Meccanica (2008) 43: 115. April 2008, Volume 43, Issue 2, pp 115–124.

[17] “Material characterization of SS 316 in low-cycle fatigue loading,” Dutta, A., Dhar, S. & Acharyya, S.K. J Mater Sci (2010) 45: 1782. April 2010, Volume 45, Issue 7, pp 1782–1789.

[18] ABAQUS (2011) “ABAQUS Documentation”, Dassault Systèmes, Providence, RI, USA.

[19] Rudolph J, Gilman T, Weitze B, Willuweit A, Kalnins A. “Using Nonlinear Kinematic Hardening Material Models for Elastic–Plastic Ratchetting Analysis.” ASME. J. Pressure Vessel Technol. 2016;138(5):051205-051205-8. doi:10.1115/1.4033092.

[20] Gilman T, Weitze B, Rudolph J, Willuweit A, Kalnins A. “Using Nonlinear Kinematic Hardening Material Models for Elastic-Plastic Ratchetting Analysis.” ASME. ASME Pressure Vessels and Piping Conference, Volume 1A: Codes and Standards ():V01AT01A046. doi:10.1115/PVP2015-45674.

[21] ASME Boiler & Pressure Vessel Code, 2013, “Section III Division 1—Subsection NB and Section VIII Division 2,” American Society of Mechanical Engineers, New York.

[22] ABAQUS Analysis User’s Manual, Materials, Chap. 23, Section 23.2, Subsection 23.2.2, Usage and Calibration of the Kinematic Hardening Models, Nonlinear isotropic/Kinematic Hardening Model, Defining the Kinematic Hardening Component by Specifying Half-Cycle Test Data.

Biography

Sirui Li received the B.Eng. degree in vehicle engineering from Beijing Institute of Technology (BIT), Beijing, China, in 2016. He is currently doing research with Professor Natasha Vermaak and working toward the M.S. degree within the Department of Mechanical Engineering and Mechanics, Lehigh University.